Physics Letters A 373 (2009) 3775–3778

Contents lists available at ScienceDirect

Physics Letters A

www.elsevier.com/locate/pla

Instabilities of Taylor columns in a rotating stratified fluid

Rainer Hollerbach

Department of Applied Mathematics, University of Leeds, Leeds, LS2 9JT, United Kingdom

ARTICLE INFO

Article history:
Received 3 June 2009
Received in revised form 4 August 2009
Accepted 12 August 2009
Available online 15 August 2009
Communicated by C.R. Doering

ABSTRACT

We numerically solve for the flow in a differentially rotating spherical shell, with a stable stratification imposed along the rotation axis. The axisymmetric basic state evolves from a Stewartson layer in the unstratified limit to a Taylor column in the strongly stratified limit. For the Taylor columns, we next compute the linear onset of non-axisymmetric instabilities, and show that small (0.1) and large (10) Prandtl numbers yield very different results. For $Pr = 10$, positive and negative differential rotations also yield fundamentally different instabilities.

One of the most familiar results in rotating fluid dynamics is the formation of Taylor columns, in which an obstacle in a flow controls the entire fluid column above and/or below it parallel to the axis of rotation [1]. Applications include the flow over topography in meteorology and oceanography [2–5].

In this work we will study a particularly simple type of Taylor column that can be set up in a differentially rotating system, such as two concentric spheres rotating about the same axis (the z axis), but with slightly different angular velocities. This is also a familiar problem in rotating fluid dynamics, and yields a so-called Stewartson layer [6] on the tangent cylinder, the cylinder that touches the inner sphere and is parallel to the z axis.

Previous work on Stewartson layers has focused on the detailed structure of the layers themselves [6–8], as well as on the non-axisymmetric instabilities that arise once the differential rotation becomes sufficiently great [9–12]. In contrast, here we will focus on the entire region inside the tangent cylinder, which one can think of as a Taylor column, induced and controlled by the differential rotation of the inner sphere.

In particular, we will consider the effect of taking the fluid to be increasingly strongly stratified along the z axis. The most basic effect of stratification on Taylor columns is well known; they no longer extend almost indefinitely in z, but instead become increasingly shortened and compressed [13]. We will map out a continuous transition from unstratified Stewartson layers that extend all the way to the outer boundary, to stratified Taylor columns that do not. Although the two limiting cases are continuously connected, we will see that their detailed structures and asymptotic scalings are quite distinct in many ways. Finally, we will compute some of the non-axisymmetric instabilities in the strongly stratified Taylor column limit, and show that they are very different from the instabilities in the unstratified Stewartson layer limit.

Consider two concentric spherical shells, with radii r_i and r_o, rotating about the z axis with rotation rates Ω_i and Ω_o, respectively. The temperature of both spheres is additionally forced to be $T = T_0 + \beta z$, where T_0 is some suitable reference temperature, and β is the imposed temperature gradient in z.

It is also explicitly worth noting that the stratification is along the *axial* direction z, not the radial direction r. Correspondingly, gravity is taken to be $\mathbf{g} = -g\hat{\mathbf{e}}_z$, as it would be in a lab experiment. If one were instead considering planetary or stellar interiors, then gravity would be radially inward, and the stratification would also be in the radial direction. The basic transition from Stewartson layers to Taylor columns is likely to be similar in both problems, but the instabilities may well be very different.

In the reference frame rotating with the outer sphere, the suitably non-dimensionalised equations are then

$$(\partial_t + Ro\,\mathbf{U}\cdot\nabla)\mathbf{U} + 2\hat{\mathbf{e}}_z \times \mathbf{U} = -\nabla p + E\nabla^2\mathbf{U} + S\Theta\hat{\mathbf{e}}_z, \tag{1}$$

$$Pr(\partial_t + Ro\,\mathbf{U}\cdot\nabla)\Theta + U_z = E\nabla^2\Theta. \tag{2}$$

The Rossby number

$$Ro = \frac{\Omega_i - \Omega_o}{\Omega_o}$$

is a measure of the differential rotation; the Ekman number

$$E = \frac{\nu}{\Omega_o r_i^2}$$

is an inverse measure of the overall rotation. Both of these parameters are the same as in the unstratified Stewartson layer problem [10,11]. (An alternative definition of the Ekman number that is often also used is $E' = \nu/\Omega_o(r_o - r_i)^2$; for the $r_i = 1$, $r_o = 6$ values used here, the two are related by $E' = E/25$.)

The Prandtl number

$$Pr = \frac{\nu}{\kappa}$$

E-mail address: rh@maths.leeds.ac.uk.

0375-9601/$ – see front matter
doi:10.1016/j.physleta.2009.08.026

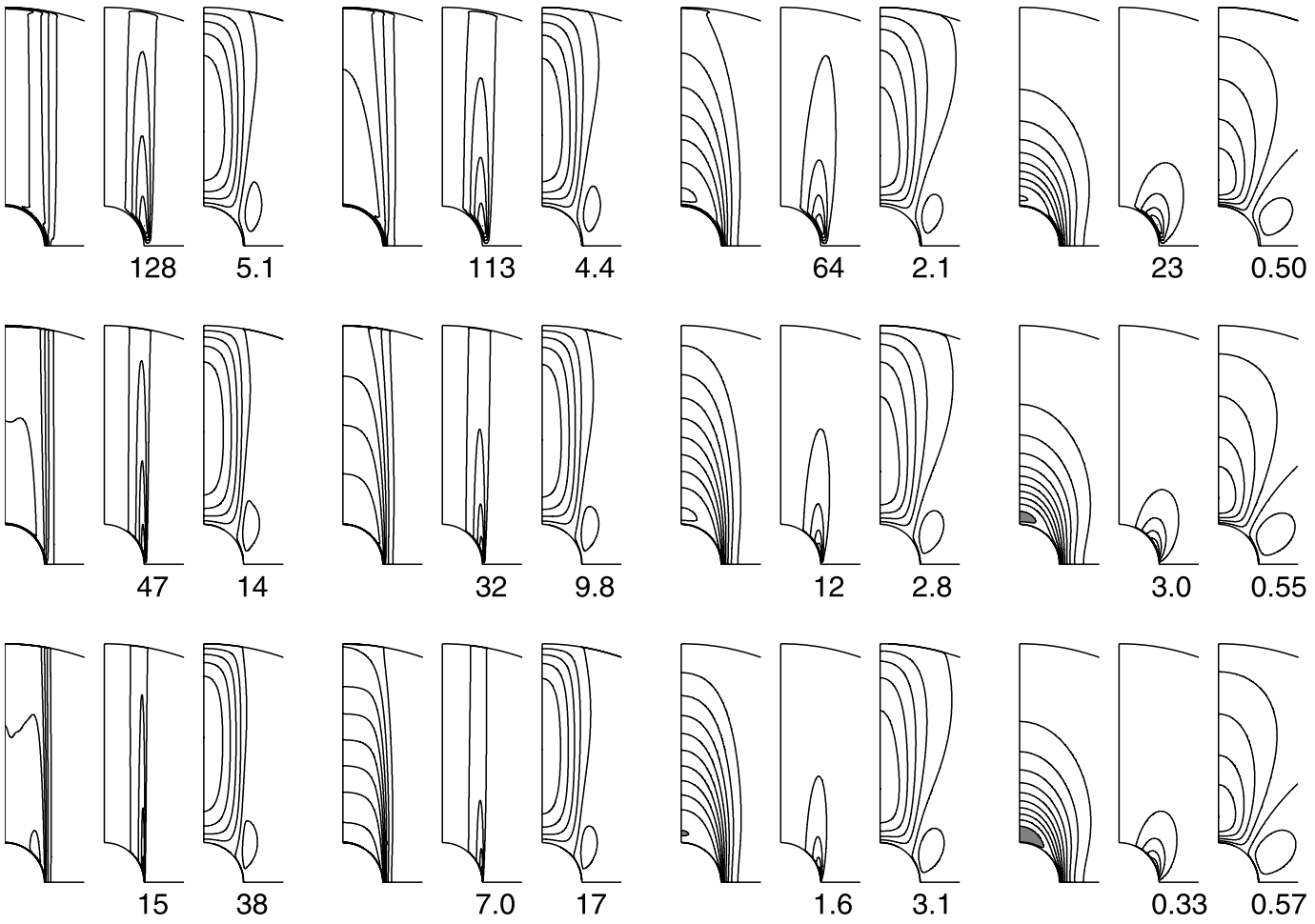

Fig. 1. Within each group of three panels, the left one shows contours of the angular velocity ω, the middle one the streamfunction of the meridional circulation ψ, and the right one Θ. The angular velocities all have contour interval 0.1, with the grey-shading in some of the plots in the fourth column denoting a slight superrotation, that is, regions where $\omega > 1$. The numbers below the ψ and Θ panels indicate values for $10^4 \cdot \psi_{\max}$ and $\Theta_{\max}$, respectively. From top to bottom the three rows correspond to $E = 10^{-3}$, 10^{-4} and 10^{-5}; from left to right $S = 10^{-3}$, 10^{-2}, 0.1 and 1 for the four groups of three panels each. Only part of the spherical shell is shown here.

is the ratio of the viscosity ν to the thermal conductivity κ, and is a material property of the given fluid. (In a lab experiment the stratification could also be achieved by using salt water of variable salinity, in which case the relevant quantity would be the ratio of viscosity to salt diffusivity, the so-called Schmidt number.)

The stratification parameter

$$S = \frac{\alpha\beta g}{\Omega_o^2} Pr,$$

where α is the thermal expansion coefficient. The quantity $\alpha\beta g$ is the square of the Brunt–Vaisala frequency, which is then normalised by the square of the rotation frequency Ω_o^2. The reason for including a factor of Pr in the definition of S will become apparent shortly.

In these equations length has been scaled by r_i, time by Ω_o^{-1}. The flow $\mathbf{U}$ is scaled by $(\Omega_i - \Omega_o) r_i$. Θ is the deviation from the imposed temperature T, scaled such that the total temperature is $T' = T_0 + \beta(z + r_i Ro\, Pr \Theta)$.

The boundary conditions on $\mathbf{U}$ are

$$\mathbf{U} = r\sin\theta \hat{\mathbf{e}}_\phi \quad \text{at } r = r_i, \qquad \mathbf{U} = \mathbf{0} \quad \text{at } r = r_o;$$

the boundary conditions on Θ are

$$\Theta = 0 \quad \text{at } r = r_i, r_o.$$

The inner and outer radii are taken to be $r_i = 1$ and $r_o = 6$. The reason for taking such a wide shell, much wider than in previous Stewartson layer calculations [10,11], is to allow sufficient space for the Taylor columns to develop, and detach from the outer boundary.

These equations and associated boundary conditions are solved numerically, using the spherical harmonics code [14]. We begin by considering the axisymmetric basic states, then we linearise about these solutions, and compute the linear onset of non-axisymmetric instabilities. Resolutions as high as 180 Legendre functions in θ and 200 Chebyshev polynomials in r were used, and were varied to check that the solutions were fully resolved.

Fig. 1 shows the axisymmetric, steady-state solutions for $E = 10^{-3}$ to 10^{-5}, $S = 10^{-3}$ to 1, and $Ro \to 0$, corresponding to an infinitesimal differential rotation of the inner sphere. Note also how the Prandtl number drops out of the governing equations (1), (2) in this $\partial_t = 0$, $Ro \to 0$ limit; the factors of Pr in the definition of S and in the scaling of Θ are included precisely in order to achieve this simplification.

Starting with $S = 10^{-3}$, the solution for $\mathbf{U}$ is essentially the familiar Stewartson layer on the tangent cylinder. The temperature deviation Θ is advected by $\mathbf{U}$, but has very little influence on it. As S is increased though, we see exactly the effect we expected, namely a gradual compression in the axial direction, until for $S = 1$ the flow forms a compact Taylor column that no longer reaches the outer boundary at all.

Table 1
Negative and positive values of Ro_c, as functions of E, for $Pr = 0.1$ and $S = 1$. All instabilities are $m = 1$ anti-symmetric, and each mode's azimuthal drift rate is indicated by the columns labelled c.

E	Ro_c	c	Ro_c	c
$4 \cdot 10^{-4}$	−0.490	−0.00689	0.559	0.01016
$2 \cdot 10^{-4}$	−0.239	−0.00366	0.260	0.00452
10^{-4}	−0.118	−0.00190	0.123	0.00211
$5 \cdot 10^{-5}$	−0.059	−0.00096	0.060	0.00102

We can also quantify somewhat more precisely just how strong the stratification must be before Θ begins to influence $\mathbf{U}$. We begin by noting that for $S = 0$, where Θ is advected completely passively, with no influence at all back on $\mathbf{U}$, the maximum values $\Theta_{\max} =$ 5.2, 15.2 and 45.6 for $E = 10^{-3}$, 10^{-4} and 10^{-5}, respectively. This $\Theta_{\max} \propto E^{-1/2}$ scaling comes about from Eq. (2), which simplifies to just $U_z = E\nabla^2\Theta$ in this $\partial_t = 0$, $Ro \to 0$ limit. Since U_z in the unstratified Stewartson layer is known to scale as $E^{1/2}$ inside the tangent cylinder [6], a $\Theta \propto E^{-1/2}$ scaling emerges quite naturally.

Next, if Θ scales as $E^{-1/2}$ in the unstratified limit, Eq. (1) suggests that it will start to influence $\mathbf{U}$ once $S \propto E^{1/2}$. To check this, we ask, how large must S be before $\Theta_{\max}$ is reduced by 10% from its original $S = 0$ value. For $E = 10^{-3}$, 10^{-4} and 10^{-5}, respectively, this 10% suppression occurs when $S = 6.3 \cdot 10^{-3}$, $1.9 \cdot 10^{-3}$ and $6.0 \cdot 10^{-4}$, in excellent agreement with the expected scaling.

Finally, turning to the strongly stratified Taylor columns at $S = 1$, we note that many of the scalings are very different from what they were in the unstratified Stewartson layer. For example, the meridional circulation evidently scales as E rather than $E^{1/2}$, and correspondingly Θ is becoming independent of E rather than scaling as $E^{-1/2}$. There is also no trace of the former Stewartson layer on the tangent cylinder. The only remaining boundary layer structure is the Ekman layer right on the inner sphere itself.

Having solved for the axisymmetric basic state, we next consider the linear onset of non-axisymmetric instabilities. Because the basic state is symmetric about the equator (perturbations of the opposite symmetry were introduced, but always decayed away), the linearised equations decouple not only into the different azimuthal wavenumbers $\exp(im\phi)$, but each wavenumber further decouples into equatorially symmetric and anti-symmetric modes, satisfying

$$\{U_r, U_\theta, U_\phi, \Theta\}(r,\theta,\phi) = \{U_r, -U_\theta, U_\phi, -\Theta\}(r,\pi-\theta,\phi),$$
$$\{U_r, U_\theta, U_\phi, \Theta\}(r,\theta,\phi) = \{-U_r, U_\theta, -U_\phi, \Theta\}(r,\pi-\theta,\phi),$$

respectively. We are then interested in computing which azimuthal wavenumber, with which equatorial symmetry, becomes unstable first, that is, for the smallest value of $|Ro|$ – where positive and negative Ro (whether the inner sphere is rotating slightly faster or slower than the outer sphere) must be considered separately, as they may yield different results. Note also that Pr no longer drops out once $Ro \neq 0$ (∂_t is also non-zero for the instabilities, which invariably drift in longitude at some speed c), so the critical Rossby numbers Ro_c will depend not just on S and E, but also on Pr. We will consider only the strongly stratified case $S = 1$, but will at least begin to map out the dependence on E and Pr.

Tables 1 and 2 show how Ro_c varies with E, for $Pr = 0.1$ and 10, respectively. For $Pr = 0.1$, positive and negative Ro are evidently rather similar; both yield an anti-symmetric $m = 1$ instability, with $Ro_c \propto E$. In contrast, for $Pr = 10$, $Ro_c \propto E^{1/2}$ for both positive and negative Ro, but the instabilities are otherwise very different, namely symmetric $m = 1$ for negative Ro, but anti-symmetric $m = 3$ for positive Ro.

To help understand these results, it is useful also to consider the energy equation associated with the linearised instability equations; one easily finds that

Table 2
Ro_c as a function of E, for $Pr = 10$ and $S = 1$. Negative Ro modes are $m = 1$ symmetric, positive Ro modes are $m = 3$ anti-symmetric.

E	Ro_c	c	Ro_c	c
$4 \cdot 10^{-4}$	−0.0439	−0.0296	0.1404	−0.00067
$2 \cdot 10^{-4}$	−0.0309	−0.0219	0.0970	−0.00039
10^{-4}	−0.0218	−0.0160	0.0674	−0.00024
$5 \cdot 10^{-5}$	−0.0153	−0.0115	0.0467	−0.00015

Table 3
Given the energy equation (3), we begin by normalising the solutions such that the total energy is 1. The column labelled (3a) then indicates in percent how the energy is divided between the two contributions $\tilde{\mathbf{U}}^2$ and $SPr\tilde{\Theta}^2$. The remaining columns show the contributions from the three integrals on the right side of (3), multiplied by 10^4 in each case.

Ro_c	(3a)	(3b) $\cdot 10^4$	(3c) $\cdot 10^4$	(3d) $\cdot 10^4$
−0.118	87/13	−17.839	28.001	−10.162
−0.059	87/13	−8.997	14.262	−5.264
0.123	86/14	−19.105	30.355	−11.252
0.060	86/14	−9.296	14.851	−5.555
−0.0218	32/68	−27.160	−3.802	30.961
−0.0153	31/69	−14.742	−2.615	17.359
0.0674	11/89	−2.161	−0.778	2.939
0.0467	11/89	−1.215	−0.502	1.716

$$\frac{d}{dt}\int \frac{1}{2}\left(\tilde{\mathbf{U}}^2 + SPr\tilde{\Theta}^2\right) dV \tag{3a}$$
$$= -E\int \left(|\nabla\times\tilde{\mathbf{U}}|^2 + S|\nabla\tilde{\Theta}|^2\right) dV \tag{3b}$$
$$+ Ro\int \mathbf{U}_0\cdot\left((\nabla\times\tilde{\mathbf{U}})\times\tilde{\mathbf{U}}\right) dV \tag{3c}$$
$$+ SPr\,Ro\int \Theta_0(\nabla\tilde{\Theta}\cdot\tilde{\mathbf{U}})\, dV, \tag{3d}$$

where $\mathbf{U}_0$ and Θ_0 are the axisymmetric basic state, and $\tilde{\mathbf{U}}$ and $\tilde{\Theta}$ the non-axisymmetric instability. We see therefore that there are two negative-definite dissipative terms, and two possible source terms, corresponding to the distinction between so-called barotropic and baroclinic instabilities [15].

Table 3 shows the various contributions to this energy equation for the eight $E = 10^{-4}$ and $5 \cdot 10^{-5}$ modes in Tables 1 and 2. We note first that the source and sink terms do indeed exactly balance, as they must, since at Ro_c the instability is neither growing nor decaying, so the energy (3a) is not changing in time. Next, probably not surprisingly, we see that for small Pr the instabilities are driven by (3c), whereas for large Pr by (3d). The other possible source term is actually a sink in every case.

Fig. 2 illustrates the spatial structure of some of these terms in (3), with the first row showing $\int(\tilde{\mathbf{U}}^2 + SPr\tilde{\Theta}^2)\, d\phi$ as a function of r and θ, that is, where the instability is concentrated in the meridional plane. The grey-shading in the second row similarly shows the relevant source terms, that is, $Ro\int \mathbf{U}_0\cdot((\nabla\times\tilde{\mathbf{U}})\times\tilde{\mathbf{U}})\, d\phi$ in the first two columns, and $SPr\,Ro\int\Theta_0(\nabla\tilde{\Theta}\cdot\tilde{\mathbf{U}})\, d\phi$ in the second two. The superimposed contours show the basic state itself, $\mathbf{U}_0$ in the first two columns, and Θ_0 in the second two.

The first two columns are very similar to one another, indicating once again that for $Pr = 0.1$, $\pm Ro$ yield much the same instability. Remembering also that these are both $m = 1$ modes, we recognise that they are essentially off-centre wobbling motions of the Taylor column. In contrast, the second two columns are quite distinct, so $\pm Ro$ yield very different instabilities when $Pm = 10$. The positive Ro mode is particularly striking, concentrated well away from the Taylor column. According to Table 3 it is also the

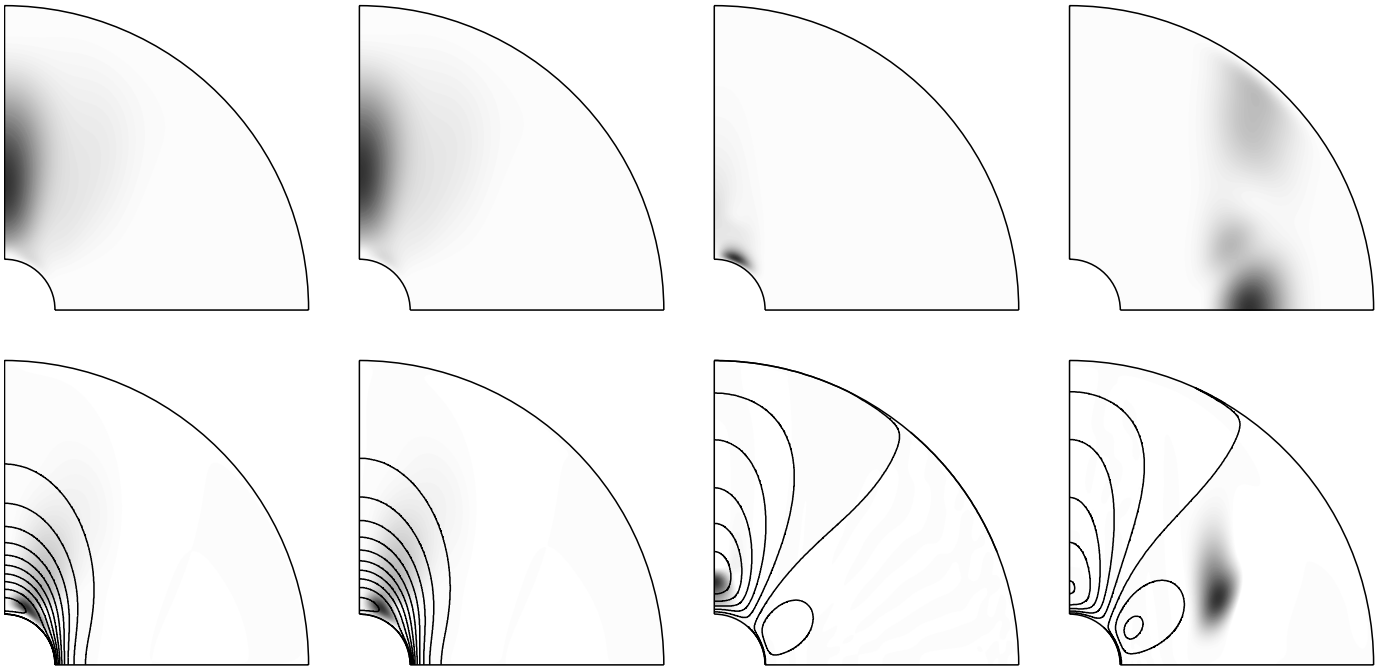

Fig. 2. From left to right, the four columns show the instabilities at ($Pr = 0.1$, $Ro_c = -0.118$), ($Pr = 0.1$, $Ro_c = 0.123$), ($Pr = 10$, $Ro_c = -0.0218$), ($Pr = 10$, $Ro_c = 0.0674$), and $E = 10^{-4}$ and $S = 1$ for all four. The top row shows $\int(\tilde{\mathbf{U}}^2 + SPr\tilde{\Theta}^2)\,d\phi$, the bottom row $\mathbf{U}_0$ and the source term (3c) for the first two, and Θ_0 and the source term (3d) for the second two.

most weakly forced of these four modes. It is an almost free strato-inertial oscillation, only very weakly forced at the edges of Θ_0.

We have thus shown that while the basic state exhibits a continuous transition from unstratified Stewartson layers to stratified Taylor columns, the instabilities are completely different from anything previously seen in the Stewartson layer problem [10,11]. The study of these Taylor column instabilities clearly deserves further attention, both theoretical and ideally also experimental.

References

[1] G.I. Taylor, Proc. R. Soc. London A 104 (1923) 213.
[2] D.L. Boyer, P.A. Davies, Annu. Rev. Fluid Mech. 32 (2000) 165.
[3] M.P. Meredith, J.L. Watkins, E.J. Murphy, N.J. Cunningham, A.G. Wood, R. Korb, M.J. Whitehouse, S.E. Thorpe, F. Vivier, Geophys. Res. Lett. 30 (2003) 2061.
[4] C. Adduce, C. Cenedese, J. Marine Res. 62 (2004) 611.
[5] G.W.K. Moore, J.L. Semple, Geophys. Res. Lett. 32 (2005) L21810.
[6] K. Stewartson, J. Fluid Mech. 26 (1966) 131.
[7] R. Hollerbach, Proc. R. Soc. London A 444 (1994) 333.
[8] E. Dormy, P. Cardin, D. Jault, Earth Planet Sci. Lett. 160 (1998) 15.
[9] W.G. Früh, P.L. Read, J. Fluid Mech. 383 (1999) 143.
[10] R. Hollerbach, J. Fluid Mech. 492 (2003) 289.
[11] R. Hollerbach, B. Futterer, T. More, C. Egbers, Theor. Comp. Fluid Dynam. 18 (2004) 197.
[12] N. Schaeffer, P. Cardin, Phys. Fluids 17 (2005) 104111.
[13] H.P. Greenspan, The Theory of Rotating Fluids, Cambridge University Press, 1968.
[14] R. Hollerbach, Int. J. Numer. Meth. Fluids 32 (2000) 773.
[15] P.D. Killworth, Dynam. Atmos. Oceans 4 (1980) 143.